



ATTENUATION OF WAVES IN PLATES AND BARS USING A GRADED IMPEDANCE INTERFACE AT EDGES

C. Vemula, A. N. Norris

Department of Mechanical and Aerospace Engineering, Rutgers University, Piscataway, NJ 08855-0909, U.S.A.

AND

G. D. Cody

Exxon Research & Engineering Co, Rt. 22 East, Annandale, NJ 08801, U.S.A.

(Received 15 May 1995, and in final form 14 February 1996)

A new method is proposed for attenuating structural wave reflections at the edges of plates and bars by using a graded impedance interface. Experimental data show that as much as 60–80% damping of energy in a 1" thick steel plate is achieved for frequencies from 2–10 kHz, using this approach. The measurements also indicate a trend towards greater damping for higher frequencies. The results observed in the experiments are explained using an S-matrix formulation based on Mindlin's theory for flexural waves. The classical, or Kirchhoff, flexural theory does not predict the observed levels of damping, indicating that shear effects are important in this attenuation mechanism. Numerical simulations indicate that the observed lower reflectivity is caused by energy dissipation within the composite material at the free end, coupled with relatively large amplitude vibrations caused by the impedance gradation.

© 1996 Academic Press Limited

1. INTRODUCTION

It is well known that energy reflection in inhomogeneous elastic materials is caused by a mismatch in the impedance properties between different regions. The free edge of a finite plate or a finite bar is an extreme case of an impedance mismatch which causes complete reflection of incident energy. A gradual change in impedance at the edges, the basic idea of a graded impedance interface, along with a damping material at the end is thus likely to reduce energy reflection. An infinite plate situation is often required in order to perform certain critical experiments in elastic wave propagation, for example experiments on Anderson localization of bending waves [1, 2]. In general, the approximation of infinite plate behavior is difficult to obtain because of the energy reflected from the boundaries. In reference [2] a minimal graded impedance interface was used to reduce the energy reflection to 50% of the incident energy. Appropriate windowing was used in order to reduce the effect of the edge reflections on the processed data. However, windowing of data is not always possible. Moreover, one would like to avoid windowing because of the spurious effects that may be introduced into the response.

In this paper we examine in detail the procedure of using graded impedance interfaces. We present results of comprehensive experiments with different types of materials used to construct efficient graded impedance interfaces. Our experimental results indicate that

when a certain type of graded impedance interface is used as much as 60–80% of the energy is damped for frequencies from 2–10 kHz. The trend indicates that even greater damping is achieved for higher frequencies. The attenuation achieved is much superior to the attenuation in the common method, e.g. reference [3], of embedding the edges in sand. It has been found that when the edges of a 1" thick steel plate are embedded in sand at most 30% of the energy is damped for frequencies above 2 kHz. Another common method is to damp energy using constrained viscoelastic layers (see, for example, references [4, 5] and other papers in the proceedings of reference [5]). This method is, however, not suitable to obtain infinite plate behaviour due to the presence of damping materials on the plate surface.

The damping of flexural energy by using graded impedance interfaces, as seen in the experiments, is a surprising result. In order to understand the mechanics underlying the observations the reflection process is modeled for a bar with graded impedance interface using two different dynamic theories: those of Kirchhoff and Mindlin, respectively. The theoretical formulation uses S-matrix reflectivity analysis, and is exact within the context of the theory considered. The comparisons between the observations and the theoretical predictions are discussed in Section 3.

2. EXPERIMENTAL SETUP AND PRELIMINARY RESULTS

2.1. EXPERIMENTAL CONFIGURATION

The experimental setup consists of a $0.61 \text{ m} \times 0.61 \text{ m} \times 2.54 \text{ cm}$ steel plate set on a $0.508 \text{ m} \times 0.508 \text{ m}$ plywood frame of 1.9 cm thickness. A thin flexible rubber tubing was placed between the frame and the plate. A Bruel & Kjaer hammer (type 8203) was used as the excitation source and the area excited was less than 1 mm². The vibration was detected using a B&K accelerometer (type 4393) mounted on a B&K magnet or using a B&K accelerometer (type 4384) mounted on a Wilcoxon magnet. The experiments were performed using the B&K 4393 accelerometer unless specified otherwise. The detector was placed at the center of the plate and the plate excited at several locations around the detector, on a circle of 1 in radius. This method has been adopted in order to measure the driving point admittance. The excitation pulse is 0.025-0.04 ms in duration, and its frequency content is flat within 10% from 0-10 kHz. The mounting resonance of the B&K 4393 accelerometer/magnet system is above 25 kHz and that of the B&K 4384 accelerometer/magnet system is at 16 kHz. The signals from both the force transducer and the accelerometer were analyzed using a dual channel signal analyzer (B&K 2032). The signal analyzer output the transfer function $H(f) = \langle a^*(f)F(f)\rangle/\langle F^*(f)F(f)\rangle$, where a(f) is the Fourier transform of the measured acceleration and F(f) is the Fourier transform of the excitation force. The angular brackets denote averaging over repeated excitation-detection measurements and * denotes complex conjugation. In general, the averaging process also reduces electronic noise.

The basic experimental parameter of concern is the driving point admittance, defined as $|H(f)/(2\pi f)|$. Figures 1 and 2 show the drive admittance for a bare plate and for a plate with its edges embedded in oil-soaked sand, respectively. There is a mounting resonance at 16 kHz in both the experiments and hence data is shown only till 10 kHz. Figures 1 and 2 also show the average value in the 2–10 kHz range, which was compared with the magnitude of the driving point admittance for an infinite plate, i.e., $(8\sqrt{D\rho h})^{-1}$ [3, 6]. The ratio is 4·3 for the bare plate, and for the plate with edges embedded in sand it is 1·74. The decrease in ratio when the edges were embedded in sand indicated

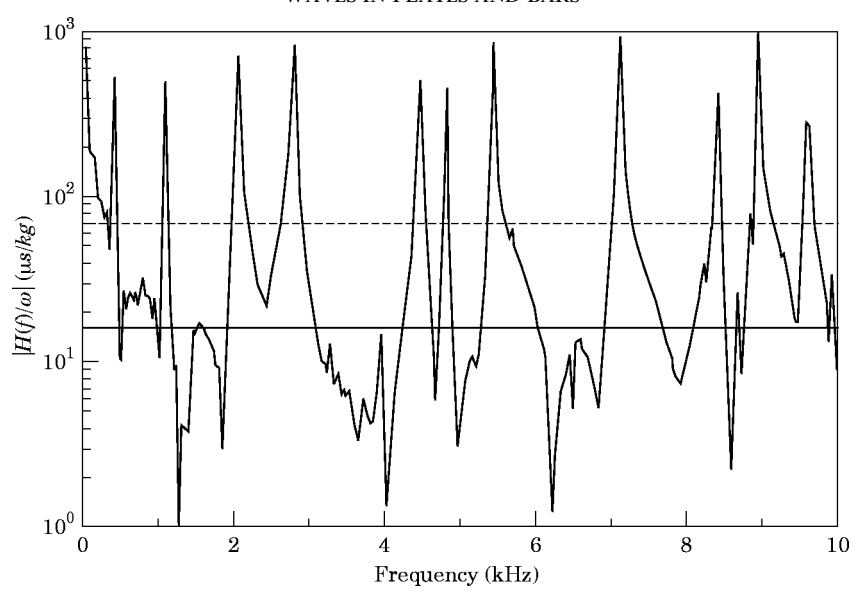


Figure 1. —, Driving point admittance at the center of a 2 ft \times 2 ft \times 1 in steel plate; ----, average of the driving point admittance for 2–10 kHz (68·76); —, driving point admittance of an infinite plate (16).

a significant damping of energy, although it is noted that distinct sharp resonant modes were still present, indicating that edge reflections are significant.

A 1-D model of waves reflecting on a finite bar is employed in order to quantify the amount of damping in the measurements. The details of the model are given below. The model estimates an effective 1-D reflection coefficient at the frequency of a specific peak by using the half-power bandwidth of the peak. It is well known that the square of the

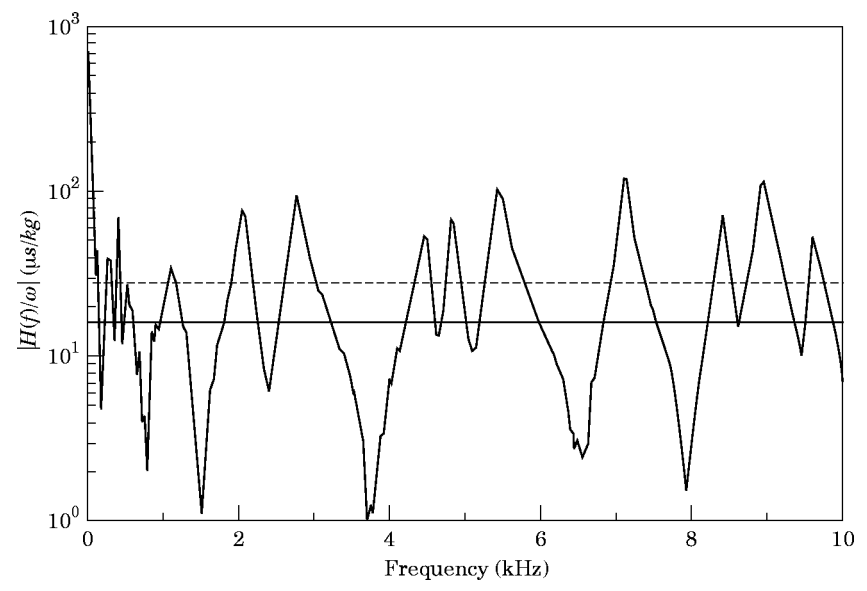


Figure 2. —, Driving point admittance at the center of a 2 ft \times 2 ft \times 1 in steel plate with edges embedded in 3 in of sand soaked in terrestic oil; ---, average of the driving point admittance for 2–10 kHz (27·78); —, driving point admittance of an infinite plate (16).

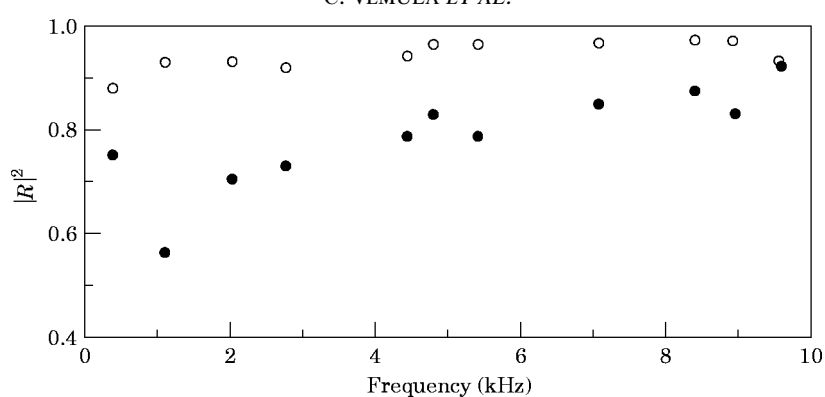


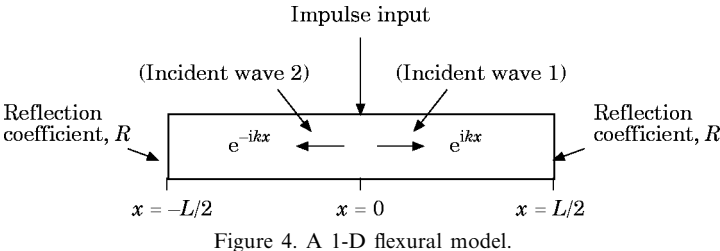
Figure 3. Reflected energy for a 2 ft \times 2 ft \times 1 in steel plate and the same plate with edges embedded in 3 in of sand soaked in terrestic oil. The two cases are: ○, bare plate; ●, plate with 3 in sand at the edges.

absolute value of reflection coefficient R gives the fraction of incident energy that is reflected. In Figure 3, $|R|^2$ is plotted for the peaks in Figures 1 and 2, where |R| is calculated using the formula derived in the next section. In Figure 3, symbols are placed at frequencies corresponding to the peaks in driving point admittance. For frequencies greater than 2 kHz it is noted that less than 30% of the incident energy is damped when the edges of a steel plate are embedded in sand. The damping in fact decreases for higher frequencies. The attenuation achieved by graded impedance interfaces is much superior as illustrated in later sections. It is noted that the present method for estimating a reflection coefficient is based on single point admittance measurements. More accurate methods exist to determine bending wave reflectivity [7, 8], using correlated intensity data from two or more accelerometers. The model described below offers an alternative procedure based upon resonance data from a single site, and is adequate for the present purposes.

2.2. 1-D REFLECTIVITY MODEL

The measured data for the drive point admittance exhibits the global effects of the system. In particular, it displays resonances associated with the modes of the finite plate or bar, which are absent in the infinite plate or bar. From the point of view of traveling waves, the resonances are caused by the multiple reflections in the system, and their strength depends strongly on the reflectivity of the edges. If there is no reflection, then there will be no modal resonances. Resonances are a sign of non-zero reflectivity. In this subsection a simple model is developed that allows interpretation of the drive point admittance in terms of an effective reflection coefficient.

The central idea is to relate the half-power bandwidth of the resonance peaks with the effective reflection coefficient at that frequency. For simplicity, a 1-D model is used for a bar under flexure, as shown in Figure 4. Time harmonic, e^{-iot}, excitation occurs at the



center of the bar, and flexural waves are radiated from the source in both directions. The radiated flexural motion comprises both a propagating wave and an evanescent wave. The reflections of the evanescent wave are small and hence are not considered. The reflection coefficient for the propagating wave is taken to be R, in general a complex quantity.

The total transverse displacement at a point on the bar is the sum of the incident wave, i.e., the wave coming directly from the source, and the multiple reflections from the edges. The displacement due to the incident wave propagating to the right and its associated multiple reflections is

$$[e^{ikx} + R e^{ik(L-x)} + R^2 e^{ik(2L+x)} + R^3 e^{ik(3L-x)} + \cdots]$$

$$= \frac{1}{1 - R^2 e^{i2kL}} e^{ikx} + \frac{R e^{ikL}}{1 - R^2 e^{i2kL}} e^{-ikx},$$
(1)

where k is the flexural wave number and L is the length of the bar. Similarly, the displacement due to the incident wave traveling to the left and its associated multiple reflections is

$$(1/(1-R^2e^{i2kL}))e^{-ikx} + (Re^{ikL}/(1-R^2e^{i2kL}))e^{ikx}.$$
 (2)

The evanescent wave to the right is ie^{-kx} and the evanescent wave to the left is ie^{kx} . The total transverse displacement at the center of the bar is then obtained by substituting x = 0 in expressions (1) and (2) and taking their sum, subtracting the contribution of one incident wave and adding the contribution of one of the evanescent waves. The ratio of the driving point admittance at the center of the bar to that for an infinite bar is thus

$$(i + (1 + R e^{ikL})/(1 - R e^{ikL}))/(i + 1)$$
 (3)

At resonance the second term in the numerator of expression (3) is much larger than the first term, and hence the magnitude is approximated by

$$\frac{1}{\sqrt{2}} \left| \frac{1 + R e^{ikL}}{1 - R e^{ikL}} \right| = \frac{1}{\sqrt{2}} \left(\frac{1 + |R|^2 + 2|R|\cos(kL - \phi)}{1 + |R|^2 - 2|R|\cos(kL - \phi)} \right)^{1/2},\tag{4}$$

where R is considered to be $|R| e^{-i\phi}$. It is clear from expression (4) that the driving point admittance at the center of a bar has peaks when $kL = 2n\pi + \phi$, $n = \pm 1, \pm 2, \cdots$. Hence, using the classical flexural wave theory to express the wavenumber k in terms of ω , it follows that to a first approximation the resonance frequencies of the bar are given by,

$$\omega_n = (2n\pi + \phi)^2 (EI/m)^{1/2}/L^2, \qquad n = \pm 1, \pm 2, \cdots.$$
 (5)

Here, m is the mass per unit length of the bar and EI is the flexural rigidity. The peak value of expression (4) is $(1/\sqrt{2}) [(1+|R|)/(1-|R|)]$, and hence at the half-power frequencies near resonance,

$$\frac{1+|R|^2+2|R|\cos{(kL-\phi)}}{1+|R|^2-2|R|\cos{(kL-\phi)}} = \frac{1}{2}\left(\frac{1+|R|}{1-|R|}\right)^2.$$
 (6)

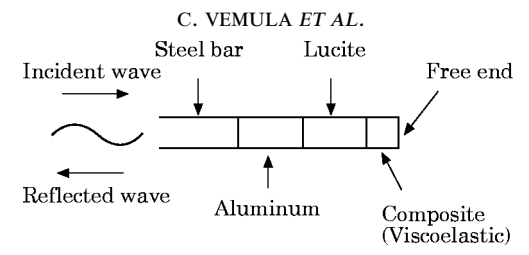


Figure 5. Graded impedance interface at the edge of a steel bar.

This simplifies to

$$kL = 2n\pi + \phi \pm \cos^{-1} Y, \qquad n = \pm 1, \pm 2, \cdots.$$
 (7)

where Y is given by

$$Y = 1 - \frac{(1 - |R|^2)^2}{6|R| - 4|R|^2 + 6|R|^3}.$$
 (8)

The frequencies associated with the half-power points follow from equation (7) as

$$\omega'_1, \omega'_2 = \omega_n + (1/L^2)(EI/m)^{1/2}[(\cos^{-1} Y)^2 \pm 2(2n\pi + \phi)\cos^{-1} Y], \quad n = \pm 1, \pm 2, \cdots$$
 (9)

The half-power bandwidth, defined as $B = (\omega_2' - \omega_1')/(2\pi)$, is therefore

$$B = 2\sqrt{\omega_n/\pi L(EI/m)^{1/4}\cos^{-1}Y}, \qquad n = \pm 1, \pm 2, \cdots.$$
 (10)

Note that the bandwidth B is a function of both the resonance frequency of the bar, ω_n , and the reflection coefficient |R|. Conversely, equation (10) can be solved to obtain |R| from the measured values of ω_n and B. This is the procedure adopted for both the plate and bar measurements.

3. GRADED IMPEDANCE INTERFACE

3.1. EXPERIMENTAL RESULTS

The materials used for the graded impedance interface were chosen so that the impedance varies gradually at the edges of a steel plate, as shown in Figure 5. The properties of the materials are given in Table 1. The properties of steel and aluminium were obtained from reference [9]. Young's modulus and shear modulus of lucite were empirically

Table 1
Properties of materials

Material	Young's modulus, <i>E</i> (GPa)	Shear modulus, μ (GPa)	Density, ρ (kg/m³)	Loss factor, η	Impedance $(\sqrt{E\rho})$ × 10 ⁶ kg m ⁻² s ⁻¹
Steel	207	80.2	7800	0.01	40.18
Aluminium	69.5	26.73	2695	0.01	13.69
Lucite	5.4	2.03	1182	0.04	2.53
Composite	0.15	0.058	1500	0.1	0.47
(Soundcoat, GP-3)					

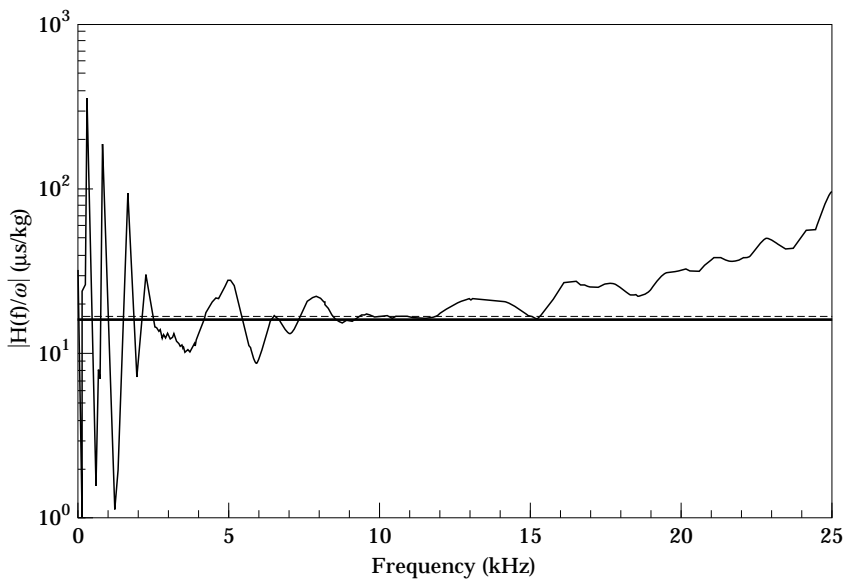


Figure 6. —, Driving point admittance at the center of a 2 ft \times 2 ft \times 1 in steel plate with 1 in \times 2 ft \times 1 in Al bars, lucite bars and 0.5 in \times 2 ft \times 1 in composite strips at the edges; —, average of the driving point admittance 2–10 kHz (16.56); —, driving point admittance of an infinite plate (16).

obtained from the natural frequencies of a block of the same material determined from experiment and finite element analysis. The loss factor of lucite is obtained from reference [10]. The composite is a viscoelastic damping material normally used for surface coating. The moduli E and μ in the plane of the composite material are known to be 0.5 GPa and 0.19 GPa, respectively, as quoted by Soundcoat, Inc. However, the moduli E and μ of the composite in the direction normal to the plane of the material are not available. The moduli normal to the plane would be lower than the moduli in the plane. The values shown in Table 1 for the composite moduli normal to plane are assumed based on empirical consistency with the Mindlin theory. The loss factor for the composite is as quoted by Soundcoat, Inc.

Experiments were performed with several different material combinations. Figure 6 shows the raw data for the driving point admittance of the steel plate when the entire graded impedance interface depicted in Figure 5 is in place on the plate edges. The gradation materials are attached at 2 ft × 1 in surfaces. Aluminium and Lucite are attached using Soundcoat B-flex epoxy and the composite is glued using Pliobond. The epoxy bond is solid at room temperature and has a damping coefficient less than that of Lucite. It is noted that for frequencies above 2 kHz the peaks are broad and the average value in the 2-10 kHz range is only 1.04 times that of the finite plate value mentioned earlier. The driving point admittance data shown in Figure 6 increases steadily above 15 kHz due to the presence of the accelerometer mounting resonance above 25 kHz. The effective reflection coefficients for the peaks, calculated using equation (10), are plotted in Figure 7. This Figure also shows the reflection coefficients obtained for reduced levels of graded impedance interface, corresponding to one or two layers. More than 60% of the energy is damped for frequencies above 2 kHz when the entire graded impedance of Figure 5 is used. The data of Figure 7 illustrate quantitatively how more damping is obtained as the level of gradation in the graded impedance interface is increased.

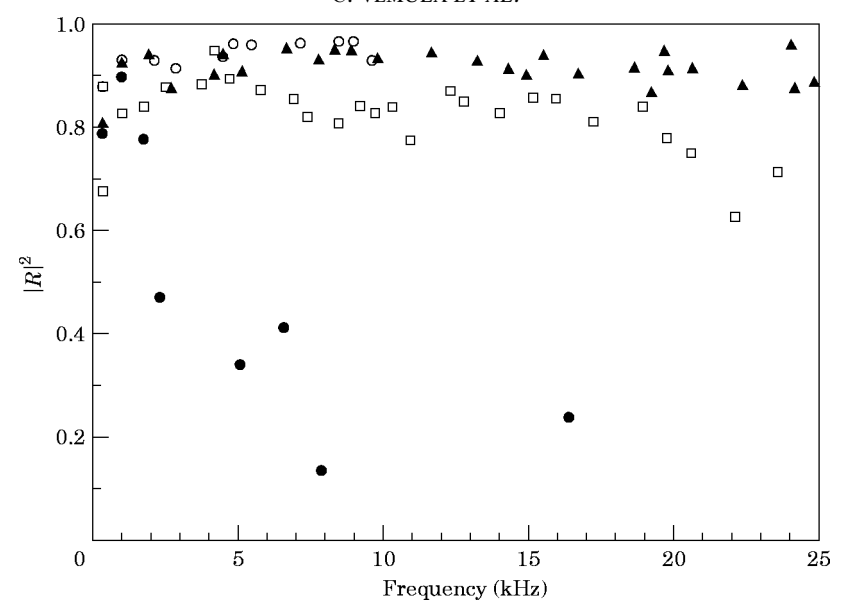


Figure 7. Reflection energy for different levels of graded impedance interface at the edges (experimental data for a $2 \text{ ft} \times 2 \text{ ft} \times 1 \text{ in steel plate}$). The four cases are: \bigcirc , bare plate; \blacktriangle , plate, Al $(1 \text{ in} \times 2 \text{ ft} \times 1 \text{ in})$; \square , plate, Al $(1 \text{ in} \times 2 \text{ ft} \times 1 \text{ in})$, Lucite $(1 \text{ in} \times 2 \text{ ft} \times 1 \text{ in})$, emposite $(0.5 \text{ in} \times 2 \text{ ft} \times 1 \text{ in})$.

The effectiveness of the graded impedance interface is further exemplified in Figure 8, which shows the reflectivity for several combinations of materials. It is noted that the composite material acts more efficiently as a damper of energy when a graded impedance

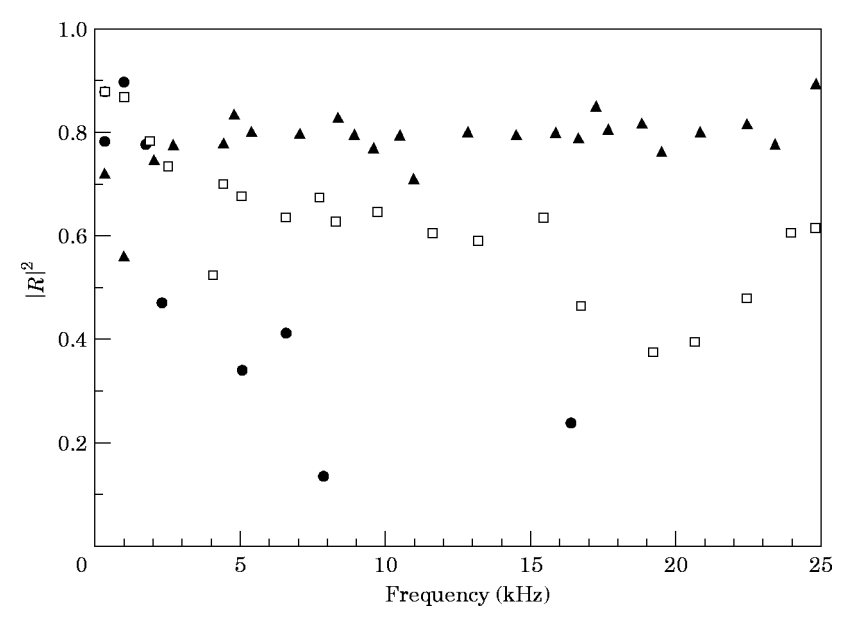


Figure 8. Reflected energy for different levels of graded impedance interface including composite, at the edges (experimental data for a 2 ft \times 2 ft \times 1 in steel plate). The three cases are: \bullet , plate, Al (1 in \times 2 ft \times 1 in), Lucite (1 in \times 2 ft \times 1 in), composite (0·5 in \times 2 ft \times 1 in); \Box , plate, Al (1 in \times 2 ft \times 1 in), composite (0·5 in \times 2 ft \times 1 in).



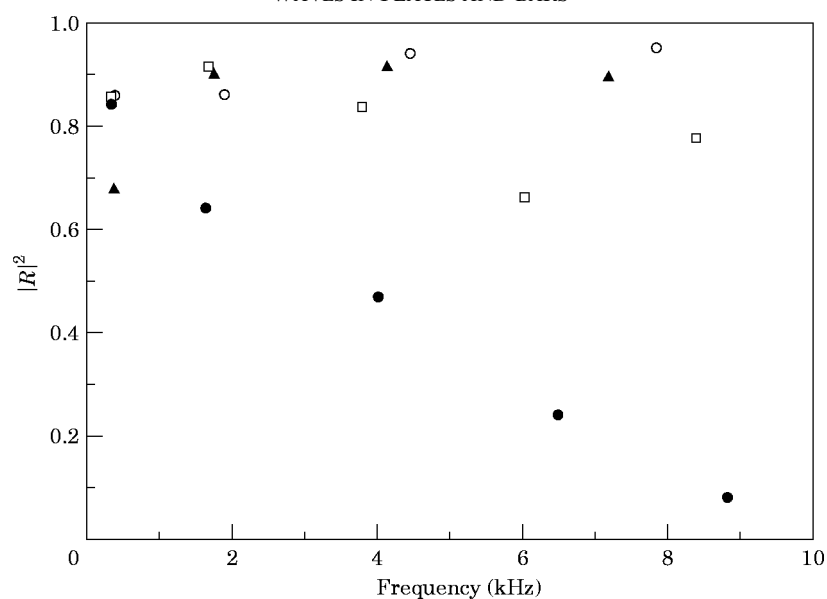


Figure 9. Reflected energy for different levels of graded impedance interface at the edges (experimental data for a 2 ft \times 1 in \times 1 in steel bar). The four cases are: \bigcirc , bare bar; \blacktriangle , bar, Al (1 in \times 1 in \times 1 in); \square , bar, Al (1 in \times 1 in \times 1 in), Lucite (1 in \times 1 in \times 1 in); \blacksquare , bar, Al (1 in \times 1 in \times 1 in), Lucite (1 in \times 1 in \times 1 in), composte (0·5 in \times 1 in \times 1 in).

interface is present. Measurement of the driving point admittance on bars yielded similar overall results as the plate. The effective reflection coefficients for bars with various graded impedance layers are shown in Figures 9 and 10. The gradation materials are attached at

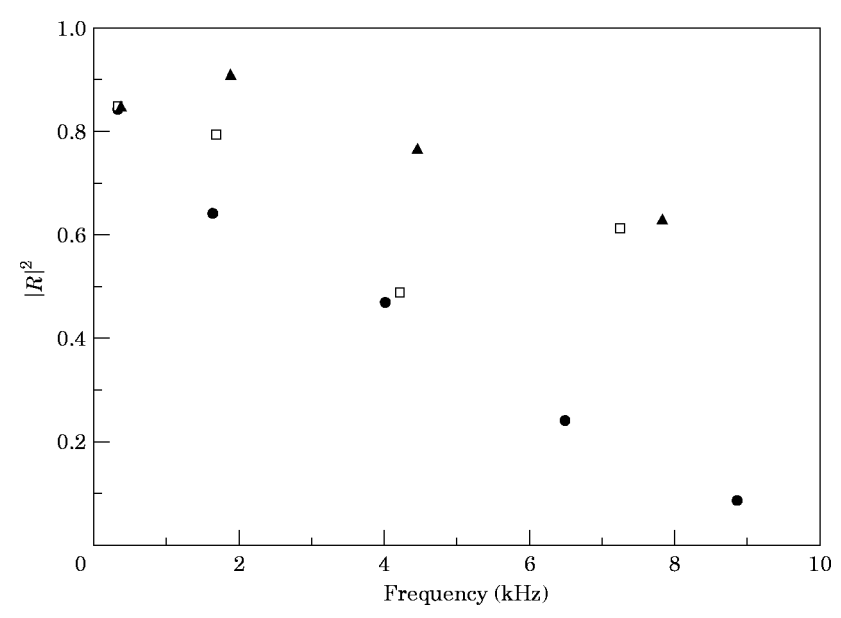


Figure 10. Reflected energy for different levels of graded impedance interface including composite, at the edges (experimental data for a 2 ft \times 1 in \times 1 in steel bar). The three cases are: \bullet , bar, Al (1 in \times 1 in \times 1 in), Lucite (1 in \times 1 in \times 1 in), composite (0·5 in \times 1 in \times 1 in); \Box , bar, Al (1 in \times 1 in \times 1 in), composite (0·5 in \times 1 in \times 1 in).

the 1 in \times 1 in ends. The mounting resonance in admittance data for bars is at 16 kHz and hence the reflection coefficients are calculated only for peaks with frequency lower than 10 kHz.

3.2. THEORETICAL DISCUSSION OF THE RESULTS

In an attempt to understand and quantify the measured data two models were considered for the bending wave reflection coefficient from the edges of a bar with different levels of graded impedance interface. The models are both one-dimensional, corresponding to reflection from the end of a semi-infinite bar with an end section of varying properties. The two flexural theories used, the Kirchhoff theory and the Mindlin theory, are briefly reviewed in Appendix A. The reflectivity analysis is performed using an S-matrix formulation for flexural waves theory, which is also explained in detail in Appendix A. The geometrical parameters are as in the experiments on bars, i.e., square cross sectional area, $1 \text{ in} \times 1 \text{ in}$.

The calculated square of the reflection coefficient is plotted in Figure 11 for the model based on Kirchhoff theory. It is significant that the Kirchhoff theory fails to predict the level of energy damping seen in experiments (as in Figure 9). The squared reflection coefficients for the model based on the Mindlin theory are compared with the corresponding experimental results in Figures 12–15 for different levels of gradation in the graded impedance interface. There is satisfactory agreement in the magnitude and the frequency dependence between the Mindlin theory results and the experimental results. The valleys observed in the Mindlin theory results, however, are not seen in the experimental results, which may be because of the few resonances in the frequency range of the valley.

The fact that the thin beam Kirchoff theory is not adequate is not surprising because of the small wavelength/thickness ratios of the materials in Table 1. At 10 kHz these range from about 6·2 for steel down to 1·5 for the composite. The major difference between the Kirchhoff and Mindlin theories is that shear effects are more accurately modeled by the latter, and it is therefore concluded that shearing motion is an important source of the energy loss in this problem.

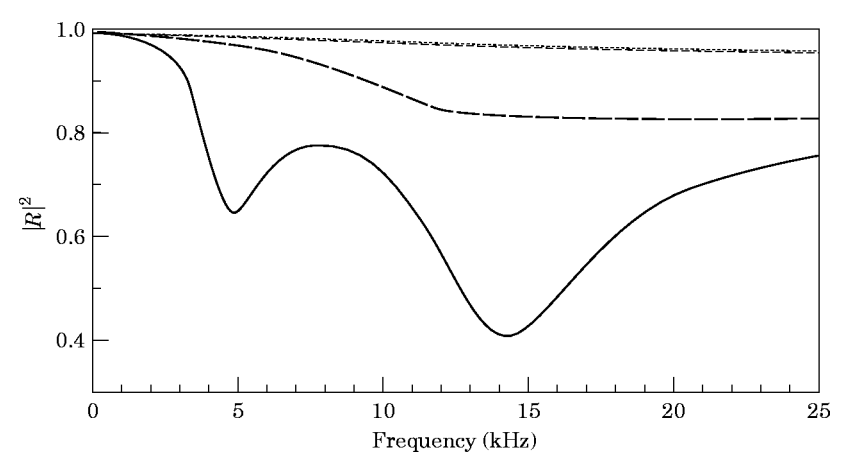


Figure 11. Reflected energy calculated using Kirchhoff theory. The four cases are: ---, steel bar $(2 \text{ ft} \times 1 \text{ in} \times 1 \text{ in})$; ----, steel bar $(2 \text{ ft} \times 1 \text{ in} \times 1 \text{ in})$, Al $(1 \text{ in} \times 1 \text{ in} \times 1 \text{ in})$; ----, steel bar $(2 \text{ ft} \times 1 \text{ in} \times 1 \text{ in})$, Al $(1 \text{ in} \times 1 \text{ in} \times 1 \text{ in})$, Lucite $(1 \text{ in} \times 1 \text{ in} \times 1 \text{ in})$; ---, steel bar $(2 \text{ ft} \times 1 \text{ in} \times 1 \text{ in})$, Al $(1 \text{ in} \times 1 \text{ in} \times 1 \text{ in})$, Lucite $(1 \text{ in} \times 1 \text{ in} \times 1 \text{ in})$; ---, steel bar $(2 \text{ ft} \times 1 \text{ in} \times 1 \text{ in})$, Al $(1 \text{ in} \times 1 \text{ in} \times 1 \text{ in})$, Lucite $(1 \text{ in} \times 1 \text{ in} \times 1 \text{ in})$, composite $(0.5 \text{ in} \times 1 \text{ in} \times 1 \text{ in})$. All the materials are attached at $1 \text{ in} \times 1 \text{ in}$ ends.

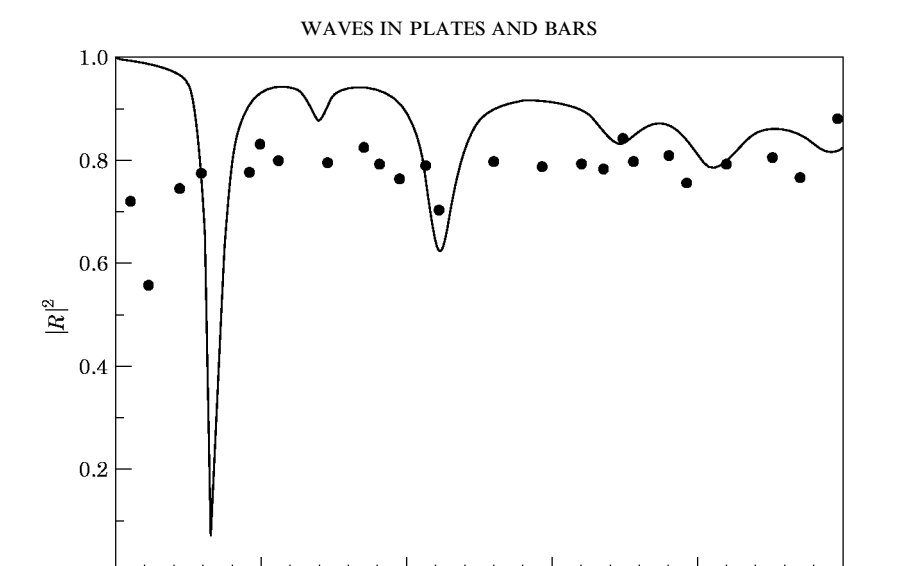


Figure 12. Reflected energy: \bullet , steel plate $(2 \text{ ft} \times 2 \text{ ft} \times 1 \text{ in})$, composite $(0.5 \text{ in} \times 2 \text{ ft} \times 1 \text{ in})$ glued at $2 \text{ ft} \times 1$ in surfaces (experiment); —, steel bar $(2 \text{ ft} \times 1 \text{ in} \times 1 \text{ in})$, composite $(0.5 \text{ in} \times 1 \text{ in} \times 1 \text{ in})$ attached at $1 \text{ in} \times 1$ in ends (Mindlin theory).

Frequency (kHz)

10

15

20

25

0

5

3.3. EFFECT OF IMPEDANCE, DENSITY AND DAMPING VARIATION IN A GRADE ON ITS REFLECTION COEFFICIENT

In order to understand better the experimentally observed phenomenon, reflectivity analysis is now performed for a steel bar (1 ft) with a graded impedance interface at the end, using the S-matrix formulation based on Mindlin flexural theory as described in

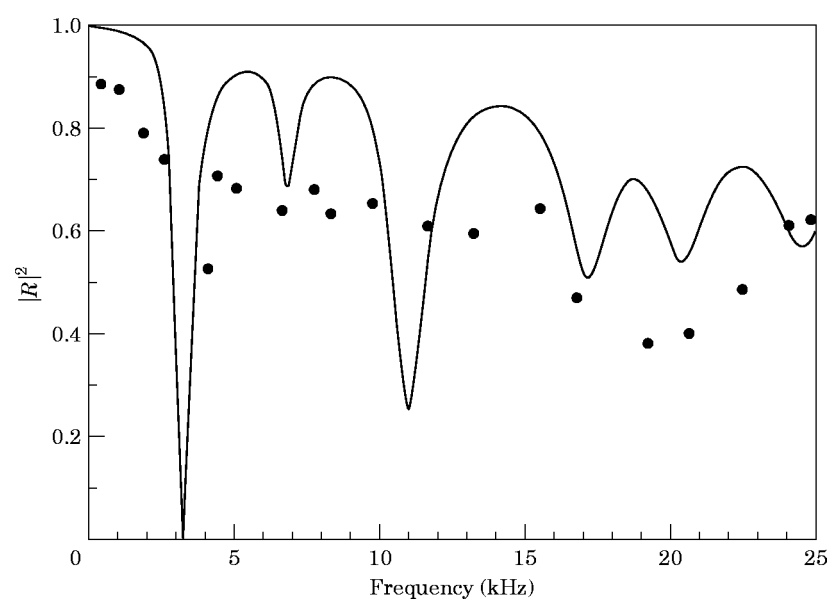


Figure 13. Reflected energy: \bullet , steel plate (2 ft × 2 ft × 1 in), Al (1 in × 2 ft × 1 in), composite (0·5 in × 2 ft × 1 in) attached at 2 ft × 1 in surfaces (experiemnt); ——, steel bar (2 ft × 1 in × 1 in), Al (1 in × 1 in × 1 in), composite (0·5 in × 1 in × 1 in) attached at 1 in × 1 in ends (Mindlin theory).

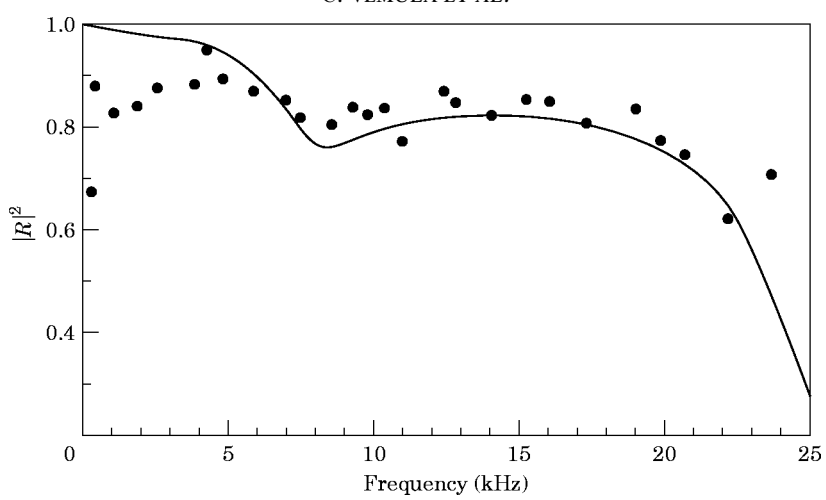


Figure 14. Reflected energy: \bullet , steel plate (2 ft × 2 ft × 1 in), Al (1 in × 2 ft × 1 in), Lucite (1 in × 2 ft × 1 in) attached at 2 ft × 1 in surfaces (experiment); ——, steel bar (2 ft × 1 in × 1 in), Al (1 in × 1 in × 1 in), Lucite (1 in × 1 in × 1 in), attached at 1 in × 1 in ends (Mindlin theory).

Appendix A. The grade is assumed to consist of 100 gradiation layers each 0.02 in in thickness and a final layer of Soundcoat GP3 composite (see Table 1), a damping material, 0.5 in in thickness. The gradation is specified by the density and impedance in each layer. The geometrical parameters are as in the experiments on bars. That is, square cross-sectional area, $1 \text{ in} \times 1 \text{ in}$. Three types of impedance variation in the grade are considered for analysis, namely, exponential decrement, linear decrement and flipped exponential decrement, as shown in Figure 16. The flipped exponential curve is obtained

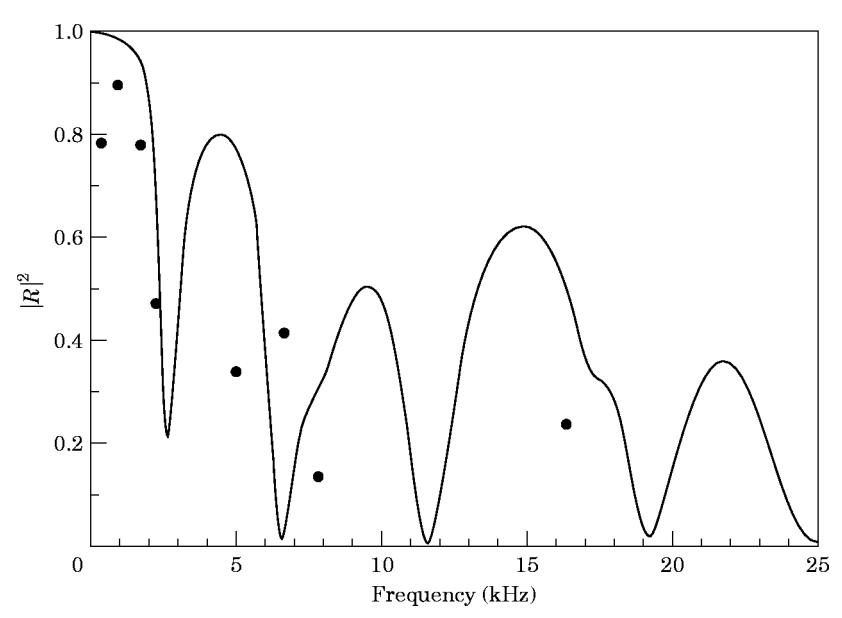
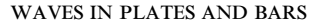


Figure 15. Reflected energy: \bullet , steel plate (2 ft × 2 ft × 1 in), Al (1 in × 2 ft × 1 in), Lucite (1 in × 2 ft × 1 in), composite (0·5 in × 2 in × 1 in) attached at 2 ft × 1 in surfaces (experiment); ——, steel bar (2 ft × 1 in × 1 in), Al (1 in × 1 in × 1 in), Lucite (1 in × 1 in × 1 in), composite (0·5 in × 1 in × 1 in), attached at 1 in × 1 in ends (Mindlin theory).



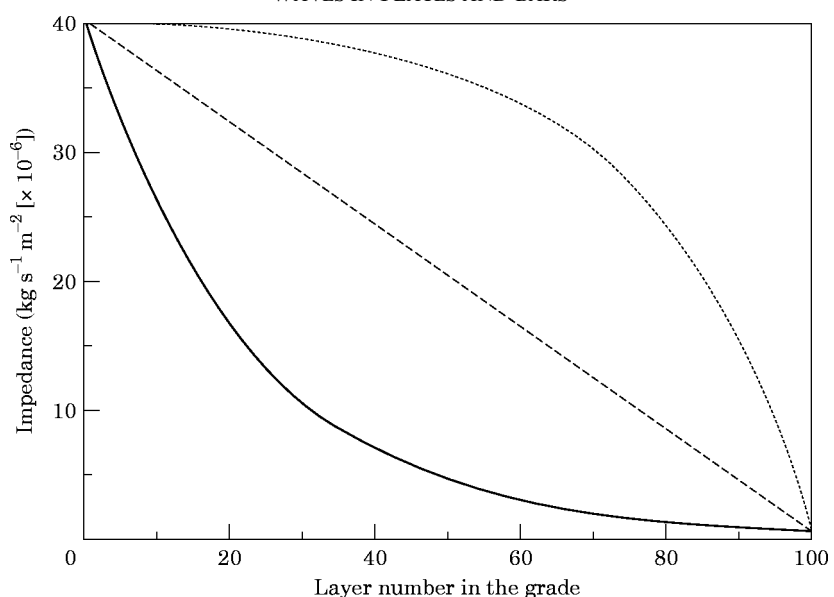


Figure 16. Impedance variation in a grade of 100 layers in between steel and composite. The three cases are:
——, exponential variation; ———, linear variation; and ----, flipped exponential variation (see text for explanation).

by flipping the exponential curve both about the linear and about the perpendicular to the linear line. The impedance of the layers in the grade varies gradually from that of steel to that of composite.

In the exponentially decreasing impedance gradation the *i*th layer impedance is $Z_0^{(1-i/101)}*Z_{101}^{(i/101)}$ where Z_0 and Z_{101} are the impedances of steel and composite, respectively. The average impedance in this grade is closer to the impedance of the composite than it is to the impedance of steel. In the linearly decreasing impedance gradation the *i*th layer impedance is $Z_0(1-i/101)+Z_{101}(i/101)$. The average impedance in this grade is equal to the average of impedances of steel and composite. In the flipped exponentially decreasing impedance gradation the *i*th layer impedance is $Z_0+Z_{101}-Z_0^{(i/101)}*Z_{101}^{(i-i/101)}$. The average impedance in this grade is closer to impedance of steel then it is to impedance of composite.

The square of the reflection coefficient based on Mindlin flexural theory is plotted in Figure 17 as a function of frequency for three grades with the types of impedance variation mentioned above. The density in all the three grades is assumed to be flipped exponentially decreasing. Damping is present only in the composite. Figure 17 indicates that the grade with exponentially decreasing impedance has the least amount of reflectivity and the grade with flipped exponentially decreasing impedance has the greatest amount of reflectivity except for a very small band of frequency. At the higher frequencies, especially, the grade exponentially decreasing impedance has significantly lower reflectivity than the grade with flipped exponentially decreasing impedance. As much as 80% of the energy is damped at higher frequencies for the grade with exponentially decreasing impedance.

The reason for lower reflectivity for a grade with exponential impedance decrement compared to a grade with flipped exponential impedance decrement is due to a larger amplitude near the free end in the former case. This fact is clearly evident if the amplitudes of the propagating waves in the layers are examined. Thus, Figure 18 shows the propagating wave amplitudes in an exponentially decreasing impedance gradation at frequency 12.58 kHz, and in a flipped exponentially decreasing impedance gradation at

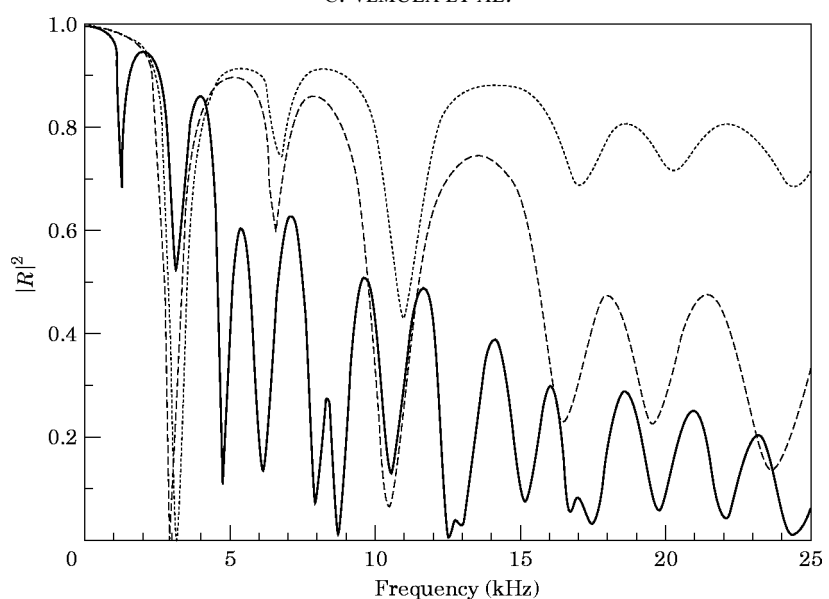


Figure 17. Reflected energy calculated using Mindlin theory for a steel bar (1 ft \times 1 in \times 1 in), grade of 100 layers (0·02 in \times 1 in \times 1 in), composite (0·5in \times 1 in \times 1 in). The density variation in the grade is of flipped exponential form. The impedance variation in the grade for the three cases is as follows: ——, exponential form; ––––, linear form; ––––, flipped exponential form. Damping is present only in the composite.

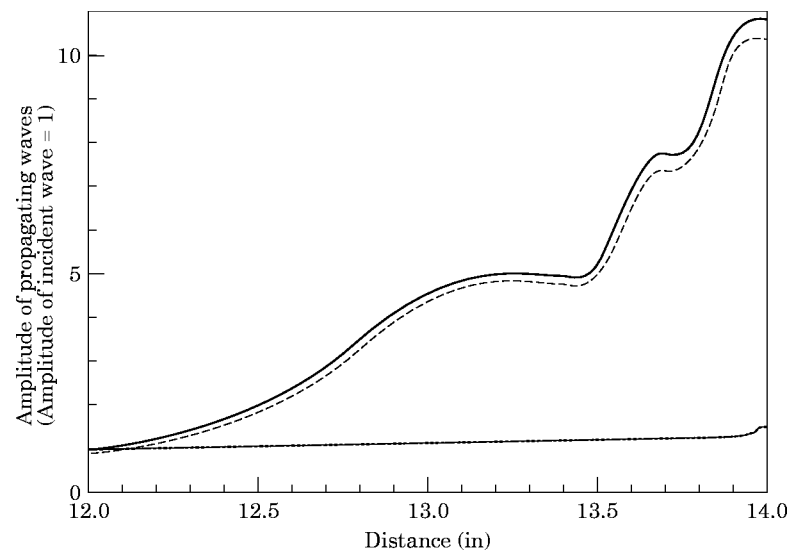


Figure 18. Amplitude of propagating waves in a steel bar $(1 \text{ ft} \times 1 \text{ in} \times 1 \text{ in})$, grade of 100 layers $(0.02 \text{ in} \times 1 \text{ in} \times 1 \text{ in})$. The density variation in the grade is of flipped exponential form. The four cases are: ——, amplitude of wave propagating in positive direction with frequency = 12.58 kHz, the impedance variation in the grade is of exponential form; ———, amplitude of wave propagating in negative direction with frequency = 12.58 kHz, the impedance variation in the grade is of exponential form; ——, amplitude of wave propagating in positive direction with frequency = 17 kHz, the impedance variation in the grade is of flipped exponential form; and ----, amplitude of wave propagating in negative direction with frequency = 17 kHz, the impedance variation in the grade is of flipped exponential form. Loss factor in the gradiation layers is same as that of steel.

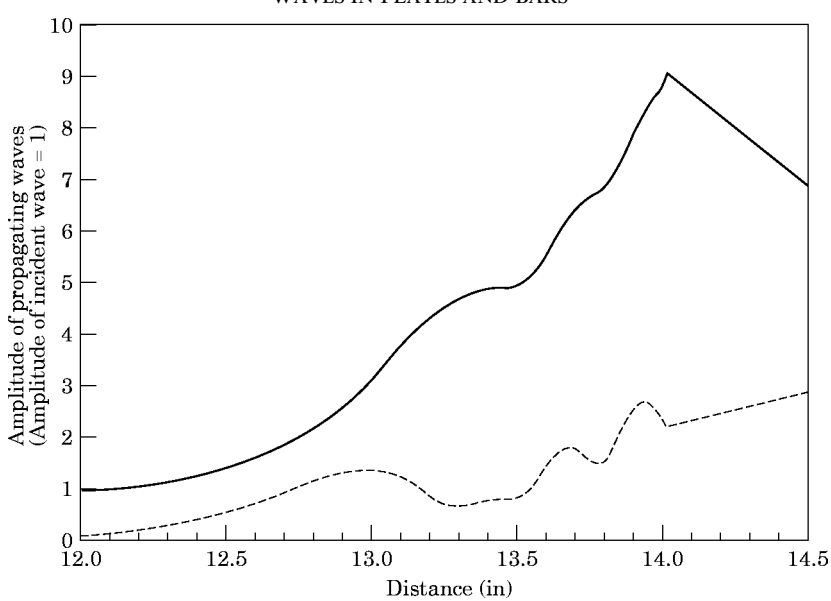


Figure 19. Amplitude of propagating waves with frequency = $12.58 \, \text{kHz}$ in a steel bar (1 ft \times 1 in \times 1 in), grade of 100 layers ($0.02 \, \text{in} \times 1 \, \text{in} \times 1 \, \text{in}$), composite ($0.5 \, \text{in} \times 1 \, \text{in} \times 1 \, \text{in}$). The impedance variation in the grade is of exponential form and the density variation is of flipped exponential form. The two cases are: ——, amplitude of wave propagating in +ve direction; ---, amplitude of wave propagating in -ve direction. Damping is present only in composite.

17.00 kHz. It is of note that the end amplitude of the former case is ten times larger than the latter. In both these cases there is no composite, and hence no source of energy dissipation, at the end. However, Figure 19 shows propagating wave amplitude at 12.58 kHz in an exponentially decreasing impedance gradiation with composite placed at the end. The amplitude of the reflection propagating wave is clearly of much smaller amplitude than the incident wave. Thus, the large amplitude at the end of the impedance gradation enables significant energy dissipation within the composite.

The effect of the density variation in a grade was analyzed for grades with the same three types of variation, shown in Figure 16, that were considered for impedance variation. It was found that there is little difference in the average reflection coefficient in a unit frequency band for the three types of gradation and hence the results are not plotted. The only significant change is in the number of peaks in the reflection coefficient curve obtained per unit frequency band. The reflection coefficient curve of flipped exponentially decreasing density gradation has the most number of peaks per unit frequency band and the reflection coefficient curve of exponentially decreasing density gradiation has the least number of peaks.

Finally, the effect of dissipation within the gradation layers was considered. A singificant effect is achievable (15% more damping) in an exponentially decreasing impedance gradation as shown in Figure 20. The two curves in Figure 20 are the reflection coefficient of an exponentially decreasing impedance grade without damping in the gradation layers and the reflection coefficient of the same grade with exponentially increasing damping variation in the gradation layers. It was found that the effect of damping in gradation layers of a linearly decreasing impedance gradation and a flipped exponentially decreasing impedance gradation is only marginal.

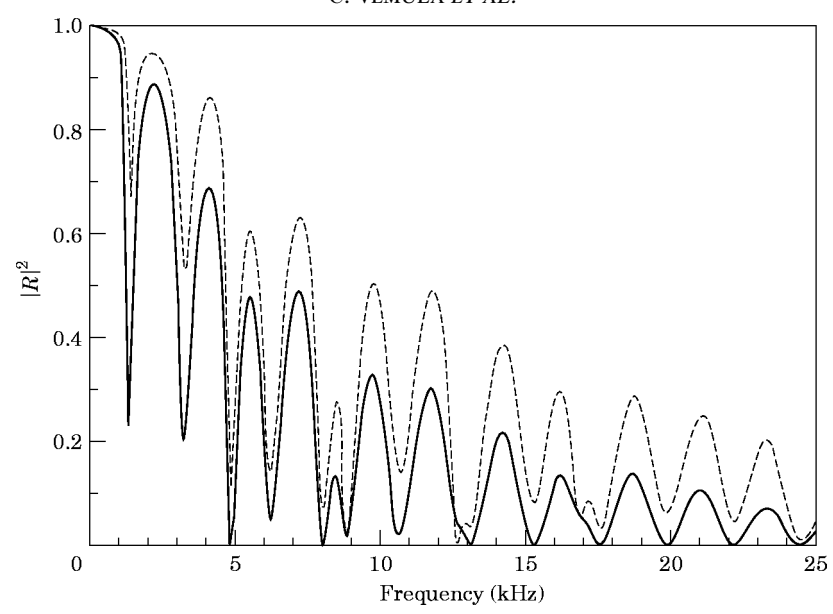


Figure 20. Reflected energy calculated using Mindlin theory for a steel bar (1 ft \times 1 in \times 1 in), grade of 100 layers (0·02 in \times 1 in \times 1 in), composite (0·5 in \times 1 in \times 1 in). The impedance variation in the grade is of exponential form and the density variation is of flipped exponential form. The two cases are: ——, loss factor in the gradation is equal to that of steel; and — —, loss factor in the gradation is exponentially increasing from that of steel to that of composite.

4. CONCLUSIONS

A graded impedance interface at the edges of plates and bars leads to a large attenuation of structural wave reflections at the edges. As much as 60–80% damping of energy is achieved in a 1 in thick steel plate for frequencies from 2–10 kHz, using one realization of this approach. The attenuation of reflected energy in this mechanism is far superior to that obtained by a viscoelastic material or sand alone at the edges. Moreover, the attenuation is achieved over a wide band of frequencies and the attenuation is in fact better for higher frequencies. This attenuation mechanism is expecially useful when the simulation of an infinite plate is desired.

The flexural vibration of a bar with a graded impedance interface at the edges is modeled both by using the Mindlin flexural theory and the Kirchhoff flexural theory along with the S-matrix formulation. It has been found that the Mindlin theory predicts the level of energy damping observed in experiments, whereas the Kirchhoff theory predicts much lesser energy damping. The shear effects are modeled more accurately in the Mindlin theory and they seem to be important in this problem.

Numerical simulations indicate that the lowered reflectivity is caused by energy dissipation within the composite material at the free end. However, the degree of energy loss is crucially enhanced by the relatively large amplitude of the freely propagating waves caused by the impedance gradation. The numerical results show that the type of impedance variation in a grade has a significant effect on the amplitude at its end. The type of density variation in a grade, however, has little effect on the average level of reflectivity. It is also possible to obtain decreased reflectivity by introducing additional damping in the gradation layers, although the damping profile must be carefully matched to the impedance variation, otherwise the effect is not appreciable. These results indicate that numerical

simulation based on Mindlin's theory can be used for the design of bending wave attenuation devices.

ACKNOWLEDGMENTS

The work of A. N. Norris was supported by the U.S. Office of Naval Research, and that of C. Vemula by Exxon Research and Engineering Co.

REFERENCES

- 1. L. YE, G. CODY, M. ZHOU, P. SHENG and A. N. NORRIS 1992 *Physical Review Letters* **69**, 3080–3083. Experimental observation of bending wave localization.
- 2. G. Cody, L. Ye, M. Zhou, P. Sheng and A. N. Norris 1993 *Photonic Band Gaps and Localization*, Edited by C. M. Soukoulis. New York: Plenum Press, Experimental observation of bending wave localization.
- 3. L. Cremer, M. Heckl and E. E. Ungar 1980 Structure-Borne Sound. Berlin: Springer-Verlag.
- 4. E. M. KERWIN 1959 J. Acoust. Soc. Am. 31, 952–962. Damping of flexural waves by a constrained viscoelastic layer.
- 5. P. S. Dubbleday 1992 Second International Congress on recent developments in air-and structure-borne sound and vibration, March 4-6, Auburn University, USA, 151-156. Analysis of constrained-layer damping of flexural and extensional waves in infinite, fluid-loaded plates.
- 6. R. Lyon 1975 Statistical Energy Analysis of Dynamical Systems: Theory and Applications. Cambridge: MIT Press.
- 7. J. LINJAMA and T. LAHTI 1992 *Journal of Sound and Vibration* **153**, 21–36. Estimation of bending wave intensity in beams using the frequency response technique.
- 8. J. LINJAMA and T. LAHTI 1993 J. Sound Vib. 161, 317–331. Measurement of bending wave reflection and impedance in a beam by the structural intensity technique.
- 9. H. L. Anderson (Editor-in-chief) 1981 A Physicist's Desk Reference. New York: American Institute of Physics.
- 10. J. D. FERRY 1980 Viscoelastic Properties of Polymers. New York: Wiley.
- 11. S. TIMOSHENKO 1940 Theory of Plates and Shells. New York: McGraw-Hill.
- 12. K. F. Graff 1991 Wave Motion in Elastic Solids. New York: Dover.
- 13. Z. Wang and A. N. Norris J. Sound Vib. 181, 457–484. Waves in cylindrical shells with circumferential submembers: a matrix approach.
- 14. B. R. MACE 1984 J. Sound Vib 97, 237-246. Wave reflection and transmission in beams.

APPENDIX A: THEORETICAL FORMULATION

A.1. KIRCHHOFF THEORY

The equations of motion for a uniform bar are well known and can be found in many textbooks, for example, Timoshenko [11]. The Kirchhoff theory models the mechanics in a bar using a single field variable, the transverse displacement, w(x, t). The solutions to the equations of motion for a time dependence of $\exp(-i\omega t)$ represent propagating waves $\exp[ik_fx]$ and $\exp[-ik_fx]$, and evanescent waves $\exp[-k_fx]$ and $\exp[k_fx]$. The flexural wave number, k_f , is

$$k_f^4 = m\omega^2/EI,\tag{A1}$$

where m is the mass per unit length and EI is the flexural rigidity of the bar. The slope is $\partial w/\partial x$ and the bending moment and the shear force are

$$M_x = -EI \partial^2 w/\partial x^2, \qquad V_x = -EI \partial^3 w/\partial x^3.$$
 (A2)

A.2. MINDLIN THEORY

The Mindlin theory models the mechanics in a bar using two variables, a rotation, $\psi(x, t)$, in addition to the transverse displacement, w(x, t). For a time dependence of $\exp(-i\omega t)$, the 1-D equations of motion reduce to [12]

$$(\partial^2/\partial x^2 + k_1^2)W_1 = 0 \qquad (\partial^2/\partial x^2 + k_2^2)w_2 = 0, \tag{A3}$$

where $w = w_1 + w_2$ is the total transverse displacement. The rotation, ψ is defined in terms of w_1 and w_2 as

$$\psi = A(k_1) \, \partial w_1 / \partial x + A(k_2) \, \partial w_2 / \partial x, \tag{A4}$$

where

$$A(k_i) = -1 + k_s^2/k_i^2, \quad j = 1, 2.$$
 (A5)

The wave numbers k_1 and k_2 are given by

$$k_{1,2}^2 = \frac{1}{2}(k_p^2 + k_s^2) \pm \sqrt{k_f^4 + \frac{1}{4}(k_p^2 - k_s^2)^2},$$
 (A6)

where

$$k_s = \omega/c_s, \qquad k_p = \omega/c_p, \qquad c_s = (\bar{\mu}/m)^{1/2}, \qquad c_p = \left[\frac{E}{\rho(1-\nu)^2}\right]^{1/2},$$
 (A7)

and k_f is as defined in equation (A1). The parameters E, ρ , and v in equation (A7) are the modulus of elasticity, density and Poisson's ratio of the material, respectively. The parameter $\bar{\mu} = \pi^2 \mu h/12$, in equation (A7), is a modified shear modulus where μ is the shear modulus and h is the thickness of the bar. The parameter $m = \rho h$, in equation (A7).

Since $k_1^2 > 0$ always, the solutions to the first equation of motion (A3) are the propagating waves $\exp[ik_1x]$ and $\exp[-ik_1x]$. The solutions to the second equation of motion (A3) are $\exp[ik_2x]$ and $\exp[-ik_2x]$, which may be either propagating or evanescing depending on whether ω is above or below the cutoff frequency, $\sqrt{12}c_s/h$, respectively. Finally, the bending moment and the shear force are

$$M_x = EI \,\partial \psi_x / \partial x, \qquad V_x = \bar{\mu} (\partial w / \partial x + \psi_x).$$
 (A8)

A.3. REFLECTIVITY ANALYSIS USING THE S-MATRIX METHOD

The S-matrix relates the waves going into a control volume and the waves coming out of the same control volume [13]. It is defined as

$$[\mathbf{V}^{\text{out}}] = [\mathbf{S}][\mathbf{V}^{\text{in}}],\tag{A9}$$

where [S] is a $2N \times 2N$ matrix [V^{out}] is a 2N-vector representing the outgoing waves and Vⁱⁿ is a vector representing the incoming waves. N is 2 for flexural waves according to either Kirchhoff or Mindlin theory. In the S-matrix formulation, distinct control volumes are identified and S-matrices are determined for each of them. The overall S-matrix is then computed from these S-matrices. For the present problem, the S-matrices are required for a junction of two different materials, for a region of uniform material, and for a free end.

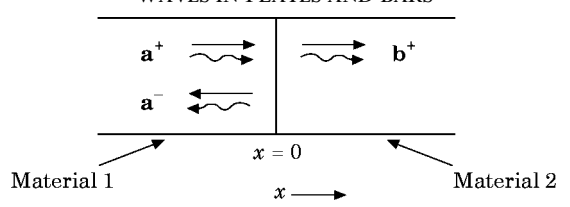


Figure 21. Waves at a junction for a wave incident from the left.

The S-matrix, $[S_T]$, for a combination of two adjacent control volumes, say A and B, whose S-matrices are $[S_A]$ and $[S_B]$ respectively, can be expressed as

$$[\mathbf{S}_{\mathbf{T}}] = [\mathbf{S}_{\mathbf{A}}] \oplus [\mathbf{S}_{\mathbf{B}}] = \begin{bmatrix} S_1^B (I - S_2^A S_3^B)^{-1} S_1^A & S_2^B + S_1^B (I - S_2^A S_3^B)^{-1} S_2^A S_4^B \\ S_3^A + S_4^A (I - S_3^B S_2^A)^{-1} S_3^B S_1^A & S_4^A (I - S_3^B S_2^A)^{-1} S_4^B \end{bmatrix}. \quad (A10)$$

The convention,

$$\mathbf{S} = \begin{bmatrix} S_1 & S_2 \\ S_3 & S_4 \end{bmatrix},\tag{A11}$$

is used in obtaining equation (A10), where S_1 , S_2 , S_3 and S_4 are $N \times N$ sub-matrices.

A.3.1. S-Matrix for a junction

At a junction, in general, there are waves incoming from both sides, and each incoming wave leads to a set of reflected waves and transmitted waves. First consider the incoming waves in the forward direction, as illustrated in Figure 21. The vectors \mathbf{a}^+ , \mathbf{b}^+ and \mathbf{a}^- in Figure 21 are *N*-vectors representing the magnitude of the incident waves, the transmitted waves and the reflected waves, respectively, and N=2. The first component in these vectors is the magnitude of the propagating wave and the second component is the magnitude of the evanescent wave, in Kirchhoff theory, and the magnitude of the wave which may be propagating or evanescing, in the Mindlin theory. The $^+$ sign indicates that a wave propagates or evanesces in the positive x-direction and the $^-$ sign indicates that a wave propagates or evanesces in the negative x-direction. The vectors \mathbf{a}^- and \mathbf{b}^+ are defined in terms of the vector \mathbf{a}^+ , using a 2 × 2 reflection matrix, $[\mathbf{R}_f]$, and a 2 × 2 transmission matrix, $[\mathbf{T}_f]$, respectively:

$$\mathbf{a}^{-} = [\mathbf{R}_f]\mathbf{a}^{+}, \qquad \mathbf{b}^{+} = [\mathbf{T}_f]\mathbf{a}^{+}. \tag{A12}$$

The subscript f in $[\mathbf{R}_f]$ and $[\mathbf{T}_f]$ indicates that these matrices are for incoming waves in the forward direction.

There are four continuity conditions at a junction, requiring that the displacement, the slope, the bending moment, and the shear force are continuous. The consequent solution for $[\mathbf{R}_f]$ and $[\mathbf{T}_f]$ when Kirchhoff theory is used is explicitly derived in reference [14]. When the Mindlin theory is used, the four continuity conditions simplify to the equations

$$\begin{bmatrix} 1 & 1 \\ k_{11}A_{11} & k_{21}A_{21} \end{bmatrix} + \begin{bmatrix} 1 & 1 \\ -k_{11}A_{11} & -k_{21}A_{21} \end{bmatrix} [\mathbf{R}_f] = \begin{bmatrix} 1 & 1 \\ k_{12}A_{12} & k_{22}A_{22} \end{bmatrix} [\mathbf{T}_f], \quad (A13)$$

$$\begin{bmatrix} k_{11}^2 A_{11} & k_{21}^2 A_{21} \\ k_{11}(1+A_{11}) & k_{21}(1+A_{21}) \end{bmatrix} + \begin{bmatrix} k_{11}^2 A_{11} & k_{21}^2 A_{21} \\ -k_{11}(1+A_{11}) & -k_{21}(1+A_{21}) \end{bmatrix} [\mathbf{R}_f]$$

$$= \begin{bmatrix} k_{12}^2 A_{12} D_2 / D_1 & k_{22}^2 A_{22} D_2 / D_1 \\ k_{12} (1 + A_{12}) \bar{\mu}_2 / \bar{\mu}_1 & k_{22} (1 + A_{22}) \bar{\mu}_2 / \bar{\mu}_1 \end{bmatrix} [\mathbf{T}_f], \tag{A14}$$

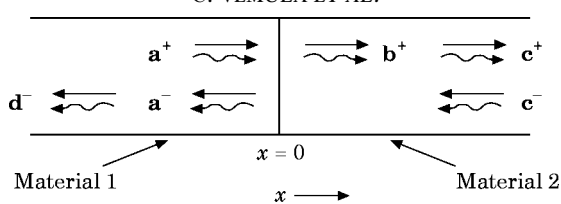


Figure 22. Waves at a junction for waves indicent from the left and the right.

where k_{ij} , i, j = 1, 2, are wave numbers, A_{ij} , i, j = 1, 2, are constants depending on the wave numbers according to equation (A5), D_i , i = 1, 2, are flexural rigidities and $\bar{\mu}_i$, i = 1, 2, are modified shear moduli, as defined previously. The first subscript in the wave numbers and in the constants depending on the wave numbers refers to the number of the wave and the second subscript refers to the material. The subscripts in the flexural rigidities and in the modified shear moduli refer to the material. The continuity conditions lead to unique solutions for $[\mathbf{R}_f]$ and $[\mathbf{T}_f]$, which are quite lengthy and hence are not written out explicitly. The reflection and transmission matrices for an incoming wave in the backward direction, $[\mathbf{R}_b]$ and $[\mathbf{T}_b]$, respectively, are evaluated using a similar procedure.

The S-matrix for a junction control volume can now be easily obtained by using the results derived so far in this section. The general case of a junction with waves incident from both sides is illustrated in Figure 22. According to the definition of the S-matrix in equation (A9), the S-matrix of a junction, $[S_{jun}]$, is determined by

$$\begin{bmatrix} \mathbf{b}^{+} + \mathbf{c}^{+} \\ \mathbf{a}^{-} + \mathbf{d}^{-} \end{bmatrix} = [\mathbf{S}_{jun}] \begin{bmatrix} \mathbf{a}^{+} \\ \mathbf{c}^{-} \end{bmatrix}. \tag{A15}$$

Using the definitions of the transmission and reflection matrices, it is easy to see that

$$[\mathbf{S}_{\text{jun}}] = \begin{bmatrix} [\mathbf{T}_f][\mathbf{R}_b] \\ [\mathbf{R}_f][\mathbf{T}_b] \end{bmatrix}. \tag{A16}$$

A.3.2. S-Matrix for a region of uniform material

The general case of a region of uniform material of length d with incoming and outgoing waves at both ends is illustrated in Figure 23. The points '1' and '2' are the end points of the control volume. The vectors \mathbf{b}^+ and \mathbf{d}^- are N-vectors representing the magnitude of the outgoing waves and the vector \mathbf{a}^+ and \mathbf{c}^- are N-vectors representing the magnitude of the incoming waves, where N=2. According to the definition of the S-matrix in equation (A9), the 2 point S-matrix, $[\mathbf{S}_{2pt}]$, is determined by

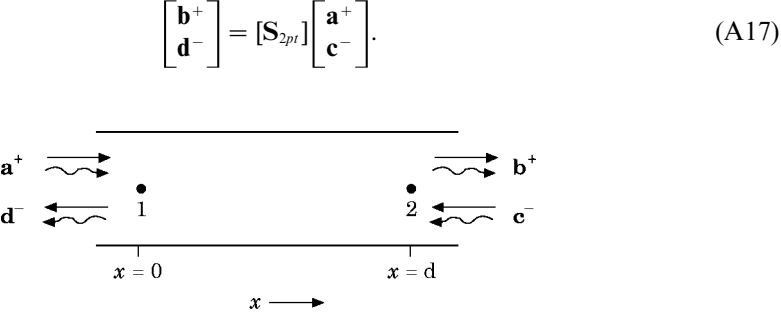


Figure 23. Waves in a region of uniform material.

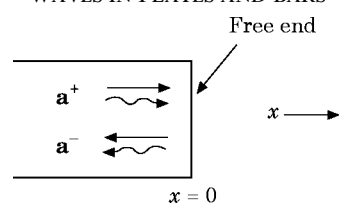


Figure 24. Waves at a free end.

Noting that the reflection matrices are zero and the transmission matrices are diagonal, it is easy to see that

$$[\mathbf{S}_{2pt}] = \begin{bmatrix} e^{ik_1d} & 0 & 0 & 0\\ 0 & e^{ik_2d} & 0 & 0\\ 0 & 0 & e^{ik_1d} & 0\\ 0 & 0 & 0 & e^{ik_2d} \end{bmatrix}.$$
(A18)

where the wave numbers k_1 and k_2 are k_f and ik_f , respectively, in Kirchhoff theory, and are given by equation (A6), for Mindlin theory.

A.3.3. S-Matrix for a free end

At a free end, as shown in Figure 24, there is an incoming wave only in the forward direction, requiring that $[\mathbf{T}_b]$ and $[\mathbf{R}_b]$ in the right hand side of equation (A16) are zero. Since all the energy is reflected, $[\mathbf{T}_f]$ is also zero, and hence, only $[\mathbf{R}_f]$ is non-zero. $[\mathbf{R}_f]$ is obtained using the boundary conditions that the bending moment and the shear force are both zero. The solution for $[\mathbf{R}_f]$, when Kirchoff theory is used, is derived in reference [14]. When the Mindlin theory is used the boundary conditions simplify to

$$\begin{bmatrix} k_{11}^2 A_{11} & k_{21}^2 A_{21} \\ k_{11}(1+A_{11}) & k_{21}(1+A_{21}) \end{bmatrix} + \begin{bmatrix} k_{11}^2 A_{11} & k_{21}^2 A_{21} \\ -k_{11}(1+A_{11}) & -k_{21}(1+A_{21}) \end{bmatrix} [\mathbf{R}_f] = 0, \quad (A19)$$

where k_{ij} and A_{ij} , i, j = 1, 2 are as defined in section A.3.1. The matrix equation (A19) is easily solved for $[\mathbf{R}_f]$. The solution, however, is not written out here explicitly due to the lengthiness of the expressions.